SUPPLEMENTAL FIGURES, LEGENDS, and METHODS

www.pnas.org/cgi/doi/10.1073/pnas.1804593115

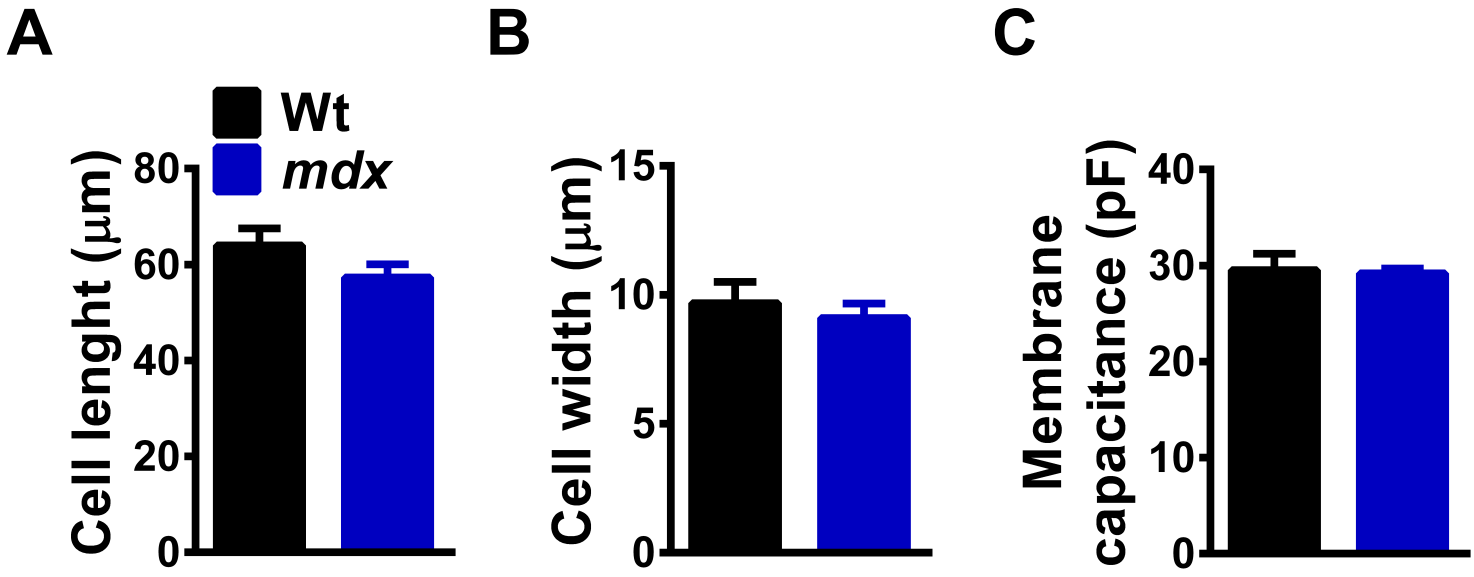

Supplemental Figure 1. SMC morphology. Freshly isolated cerebral artery SMCs from wild-type (Wt) and *mdx* mice showed no difference in length (A), width (B) (n = 10 cells/group, 3 animals/group), or membrane capacitance (C). Membrane capacitance data were obtained from SMCs that had been patch-clamped to record whole-cell K^+ currents (n = 7 cells/group, 3 animals/group). There were no significant differences.

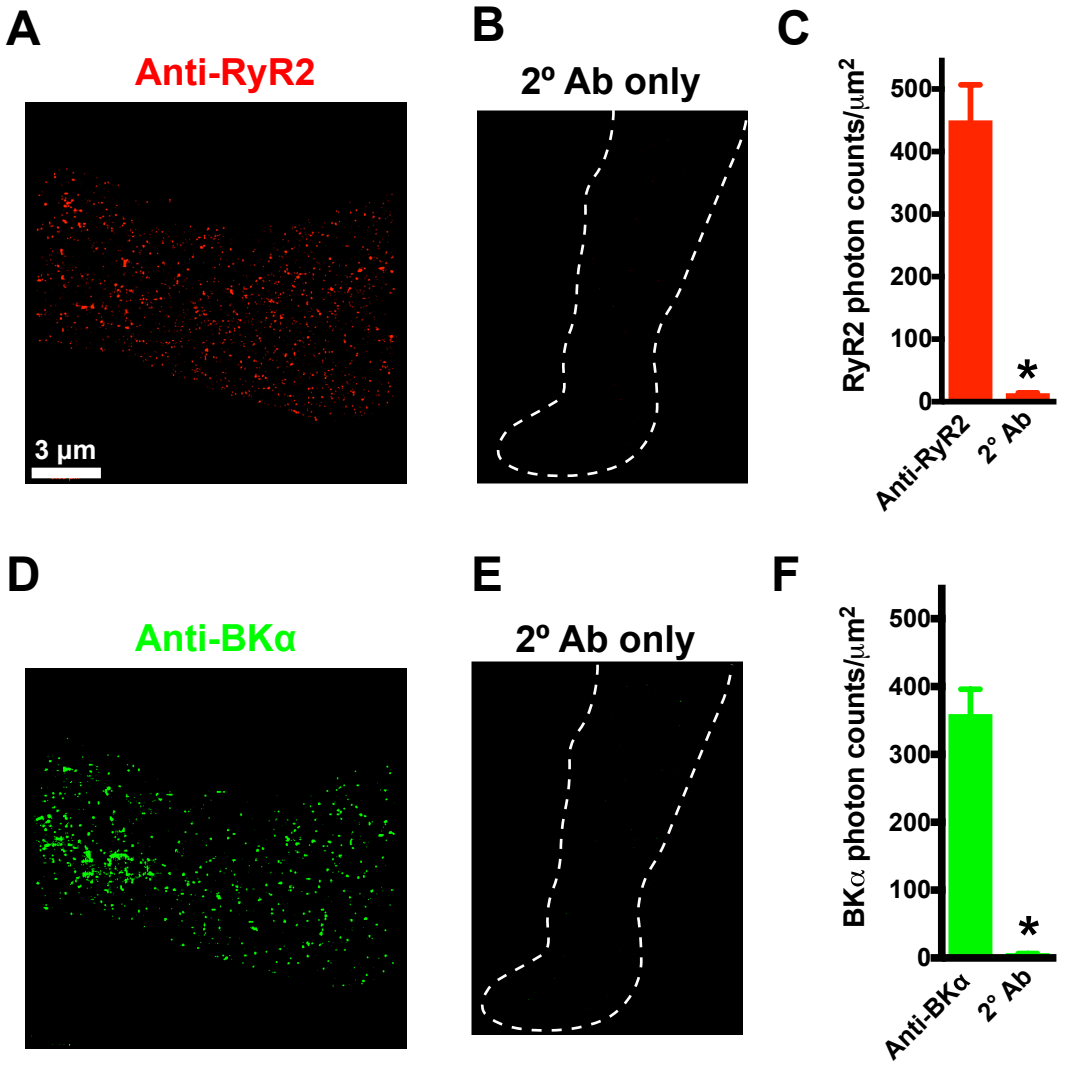

Supplemental Figure 2. Validation of RyR2 and BKα primary antibodies. (A) Super-resolution images of RyR2 (red) in a cerebral artery smooth muscle cell (SMC) exposed to RyR2 primary and corresponding secondary antibodies. (B) Image of a cerebral artey SMC exposed to secondary antibody only. (C) Summary data for mean ± SEM photon counts/µm^2 counts for these images. (D) Super-resolution images of BKα (green) in a cerebral artery SMC exposed to BKα primary and corresponding secondary antibodies. (E) Image of a cerebral artey SMC exposed to secondary antibody only. (F) Summary data for mean ± SEM photon counts/µm^2 for these images. n=8-10 cells per group. *P≤ 0.05.

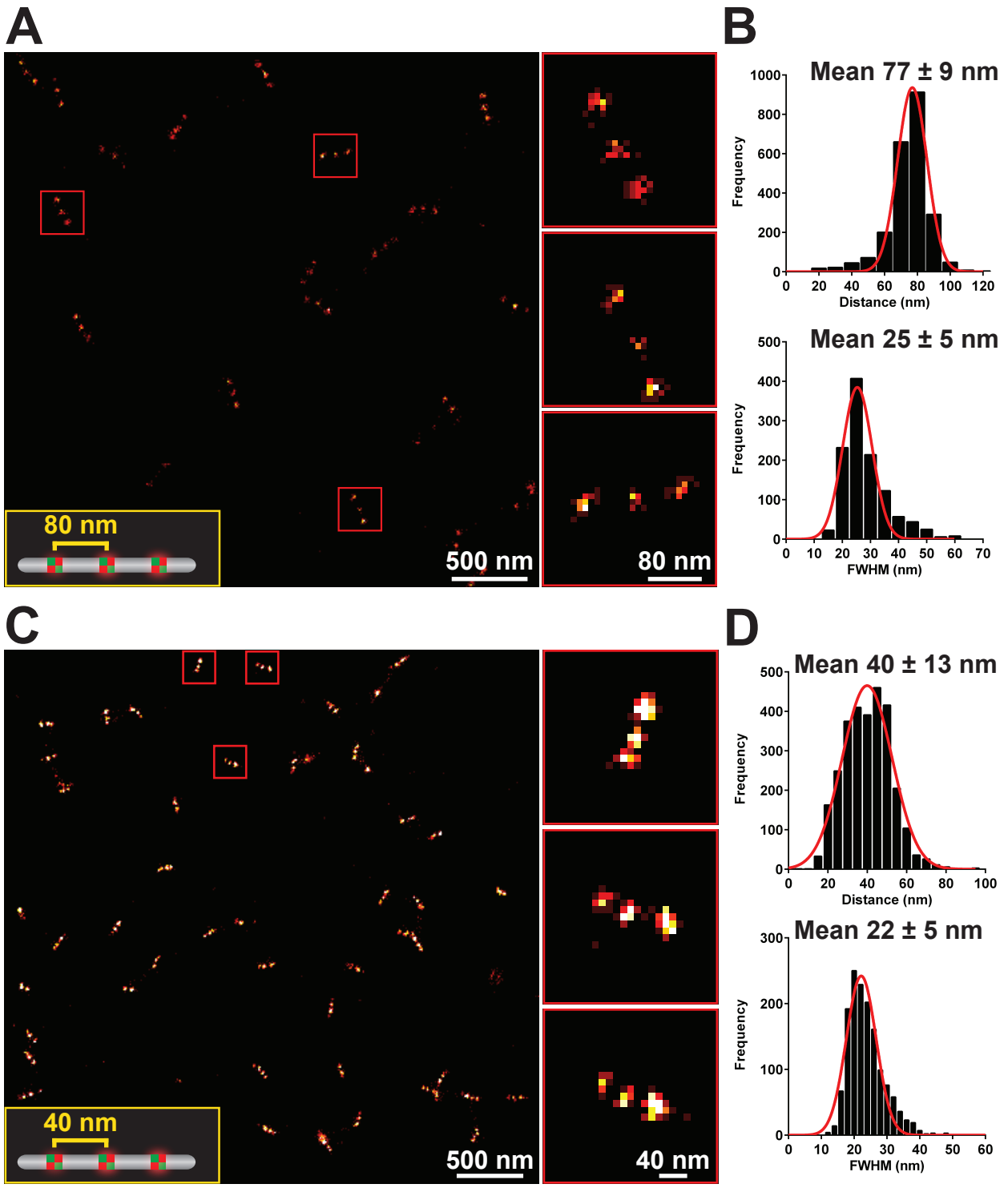

Supplemental Figure 3. Localization accuracy of GSD super-resolution. A. Super-resolution localization map of GATTA-PAINT 80RG nanorulers in the red channel (ATTO 655). The illustration in the bottom left displays the structure of a GATTA-PAINT 80RG nanoruler, with three ATTO 655 and ATTO 542 fluorophore-binding sites spaced 80 nm apart. The three regions of interest (red boxes) show individual nanorulers at an expanded scale. B. Frequency distribution of the distance between fluorophres (n = 2288) and of the full width at half maximum (FWHM) for individual fluorophores (n = 1144). Data are mean ± SD. C. Super-resolution localization map of GATTA-PAINT 40RG nanorulers in the red channel (ATTO 655). The illustration in the bottom left displays the structure of a GATTA-PAINT 40RG nanoruler, with three ATTO 655 and ATTO 542 fluorophore-binding sites spaced 40 nm apart. The three regions of interest (red boxes) show individual nanorulers at an expanded scale. D. Frequency distribution of the distance between fluorophres (n = 2893) and of the full width at half maximum (FWHM) for individual fluorophores (n = 1448). Data are mean ± SD.

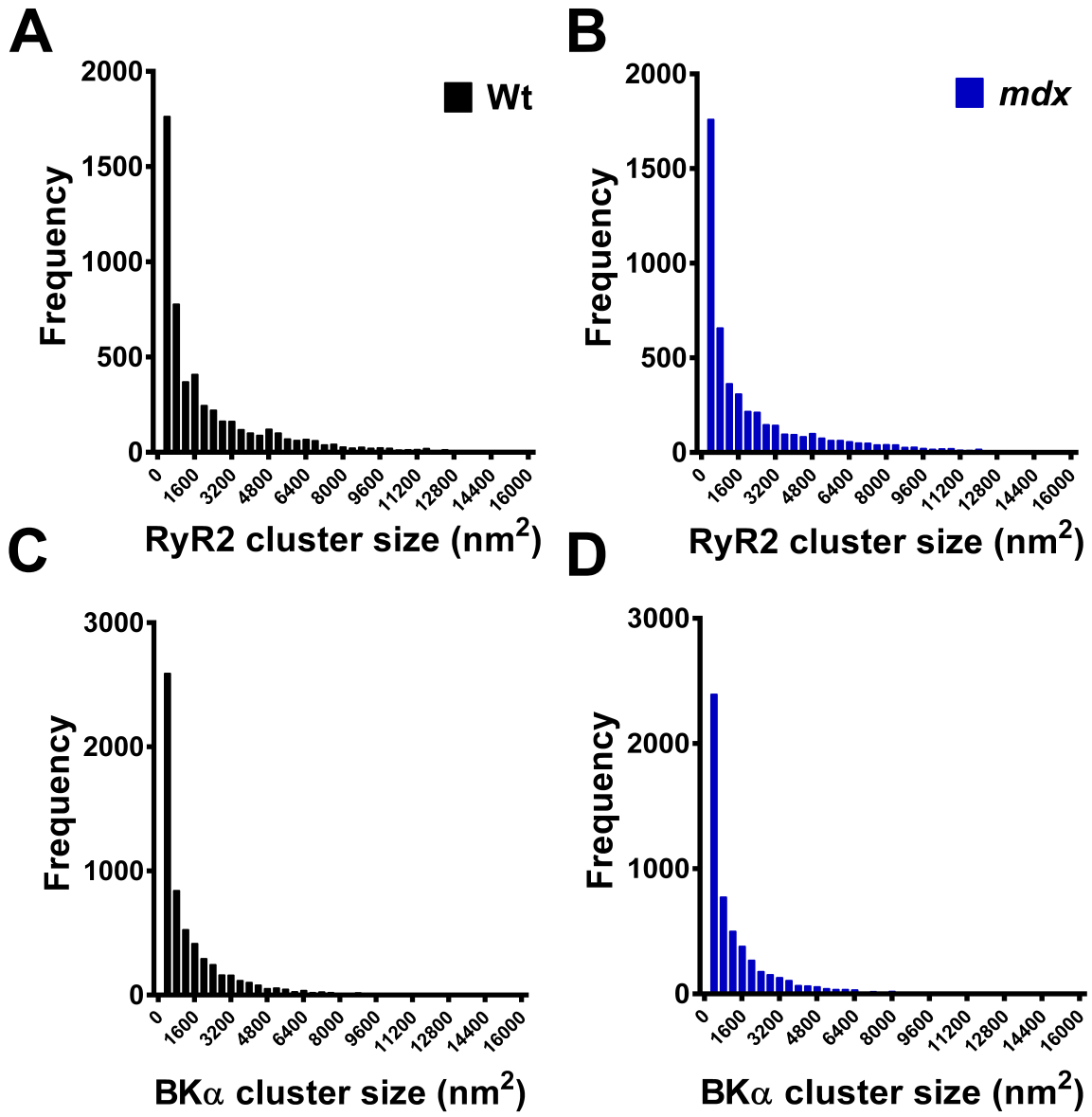

Supplemental Figure 4. Distribution RyR2 and BKα protein cluster sizes. (A and B) Histograms of RyR2 cluster size in SMCs from wild-type (Wt) (A) and *mdx* (B) mice (3,251–3,560 clusters, n = 10 cells/group, 3 animals/group). (C and D) Histograms of BKα cluster size in SMCs from Wt (C) and *mdx* (D) mice (5,390–5,960 clusters, n = 10 cells/group, 3 animals/group).

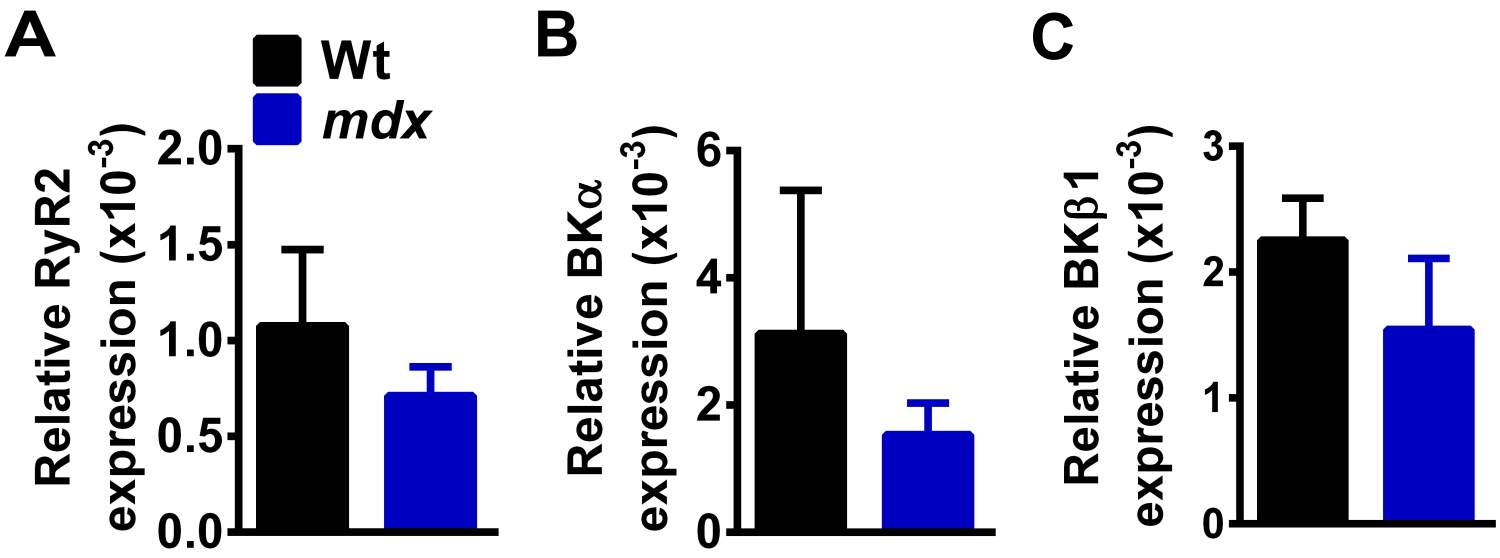

Supplemental Figure 5. RyR2 (*Ryr2*), BKα (*Kcnma1*), and BKβ1 (*Kcnmb1*) mRNA levels. Relative mRNA expression levels determined by qRT-PCR for RyR2 (A), BKα (B) and BKβ1 (C) in whole cerebral arteries from wild-type (Wt) and *mdx* mice (n = 3 mRNA isolations/group, 3 animals/group). There were no significant differences.

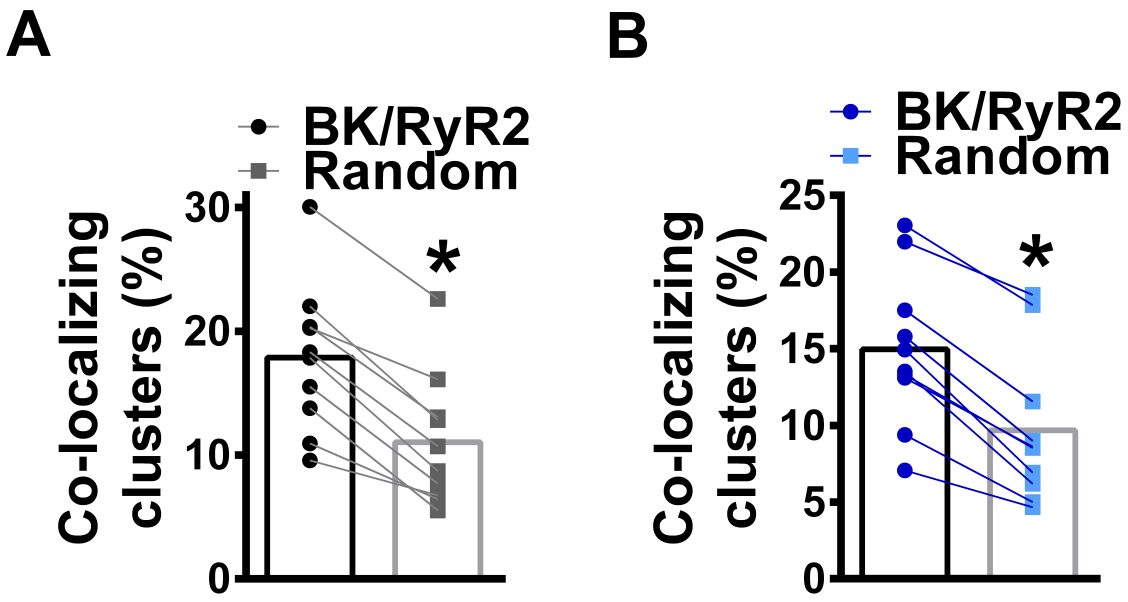

Supplemental Figure 6. Selective colocalization of RyR2 and BKα channel protein clusters in SMCs. (A) Object-based image analysis (OBA) of super-resolution localization maps obtained from co-immunolabeled SMCs from wild-type (Wt) mice versus a randomized version of the same images (n = 10 cells/group; *P < 0.05). (B) OBA of super-resolution localization maps obtained from co-immunolabeled SMCs from *mdx* mice versus a randomized version of the same images (n =10 cells/group; *P < 0.05).

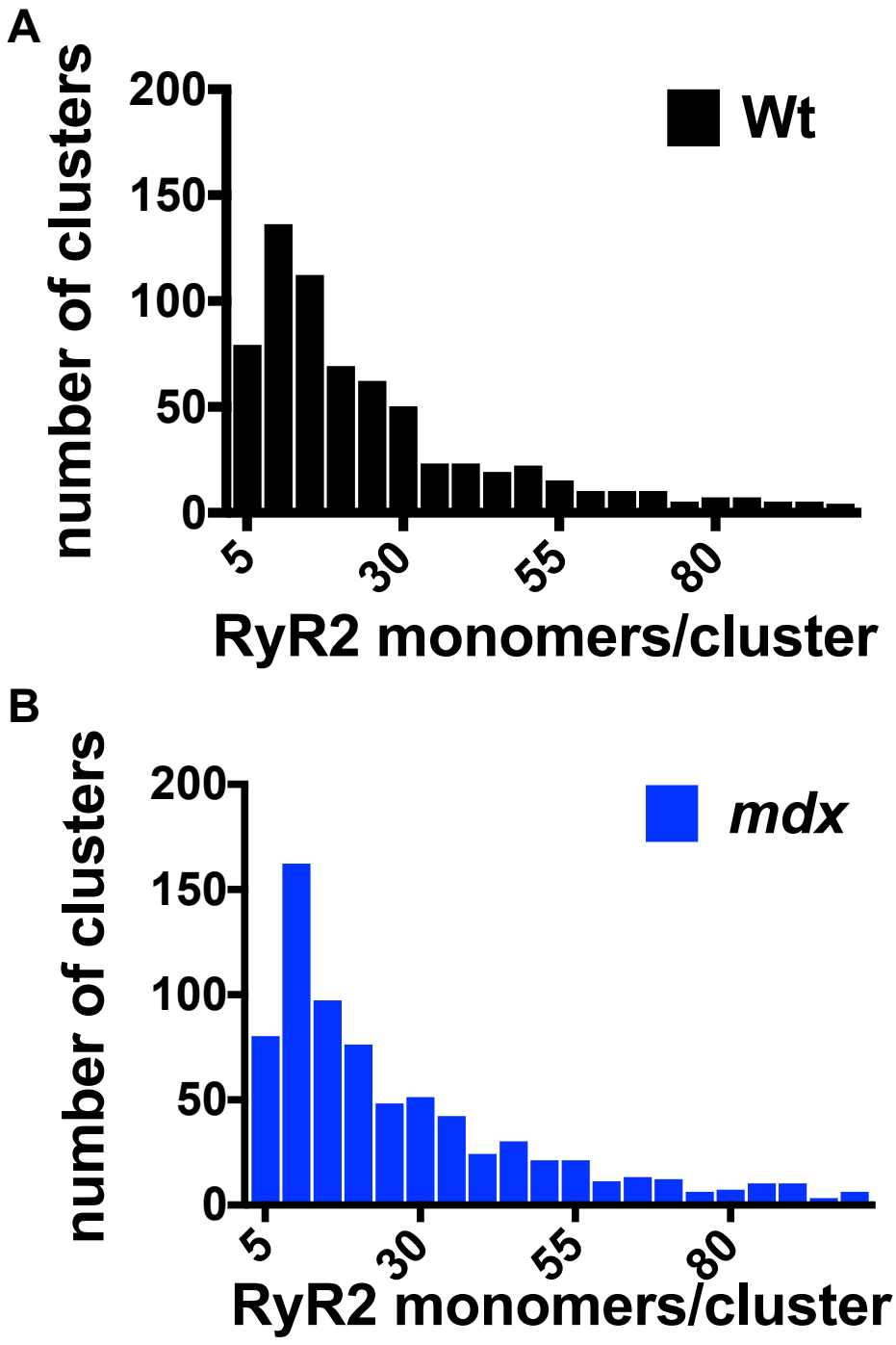

Supplemental Figure 7 - RyR2 monomers/cluster. Estimated upper limit of RyR2 monomers/cluster for cerebral artery smooth muscle cells from (A) Wild-type and (B) *mdx* mice

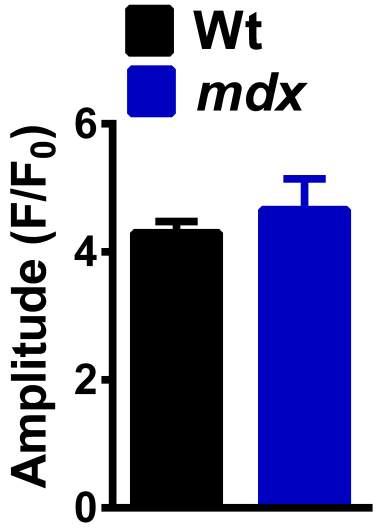

Supplemental Figure 8. SR Ca^{2+} store loads do not differ between cerebral artery SMCs from Wt and *mdx* mice. Cerebral artery SMCs isolated from wild-type (Wt) and *mdx* mice were loaded with Fluo-4-AM and imaged using high-speed confocal microscopy. Caffeine (5 mM) was applied to release SR Ca^{2+} stores. There was no difference between groups in the mean amplitude (F/F_0) of the Ca^{2+} transient induced by this treatment (n = 6 cells/group, 3 animals/group).

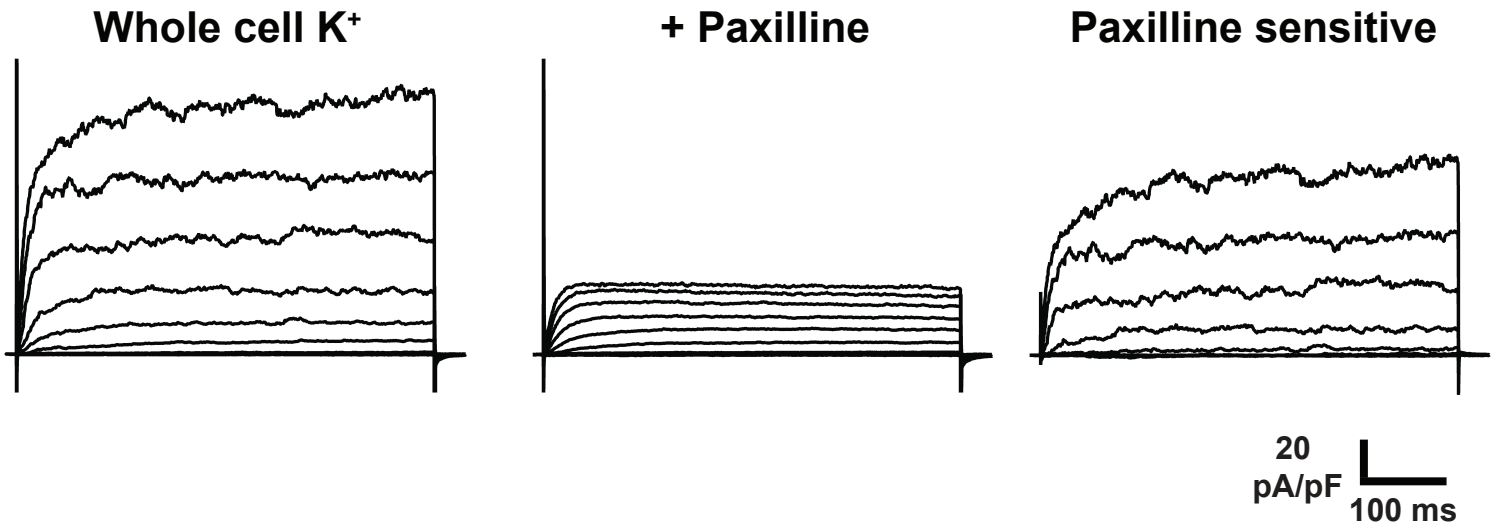

Supplemental Figure 9. Isolation of whole-cell BK currents. Representative traces of K^+ currents recorded from a SMC patch-clamped in the conventional whole-cell configuration over a range of voltage steps from -100 to +100 mV (20-mV increments) before and after administration of the selective BK channel inhibitor paxilline (1 μM). The paxilline-sensitive component was isolated by current subtraction.

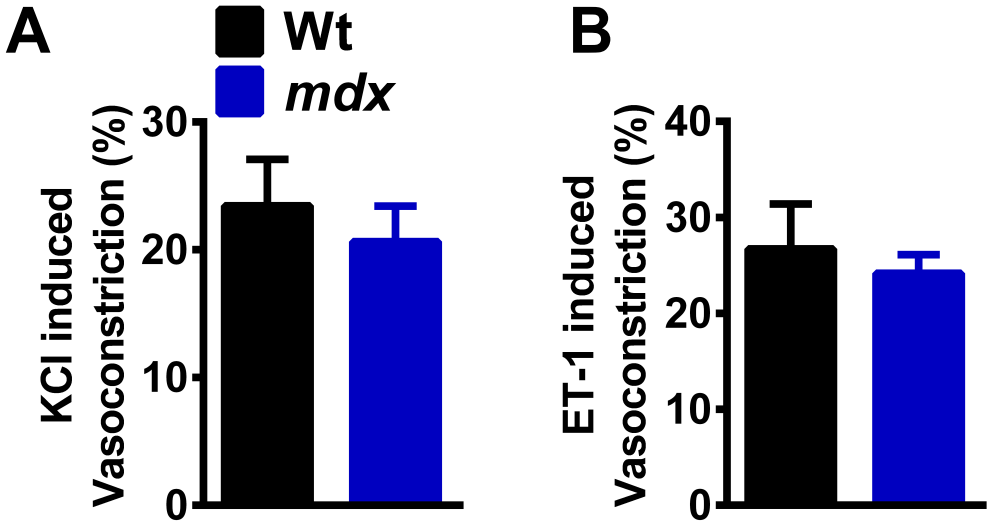

Supplemental Figure 10. Constrictor responses of cerebral pial arteries and parenchymal arterioles. (A and B) Constriction of isolated cerebral pial arteries from wild-type (Wt) and *mdx* mice in response to elevated extracellular [K^+] (60 mM) (n = 12 arteries/group, 6 animals/group) (A) and endothelin-1 (ET-1; 30 nM) (n = 6 arteries/group; 3 animals/group) (B). There were no significant differences.

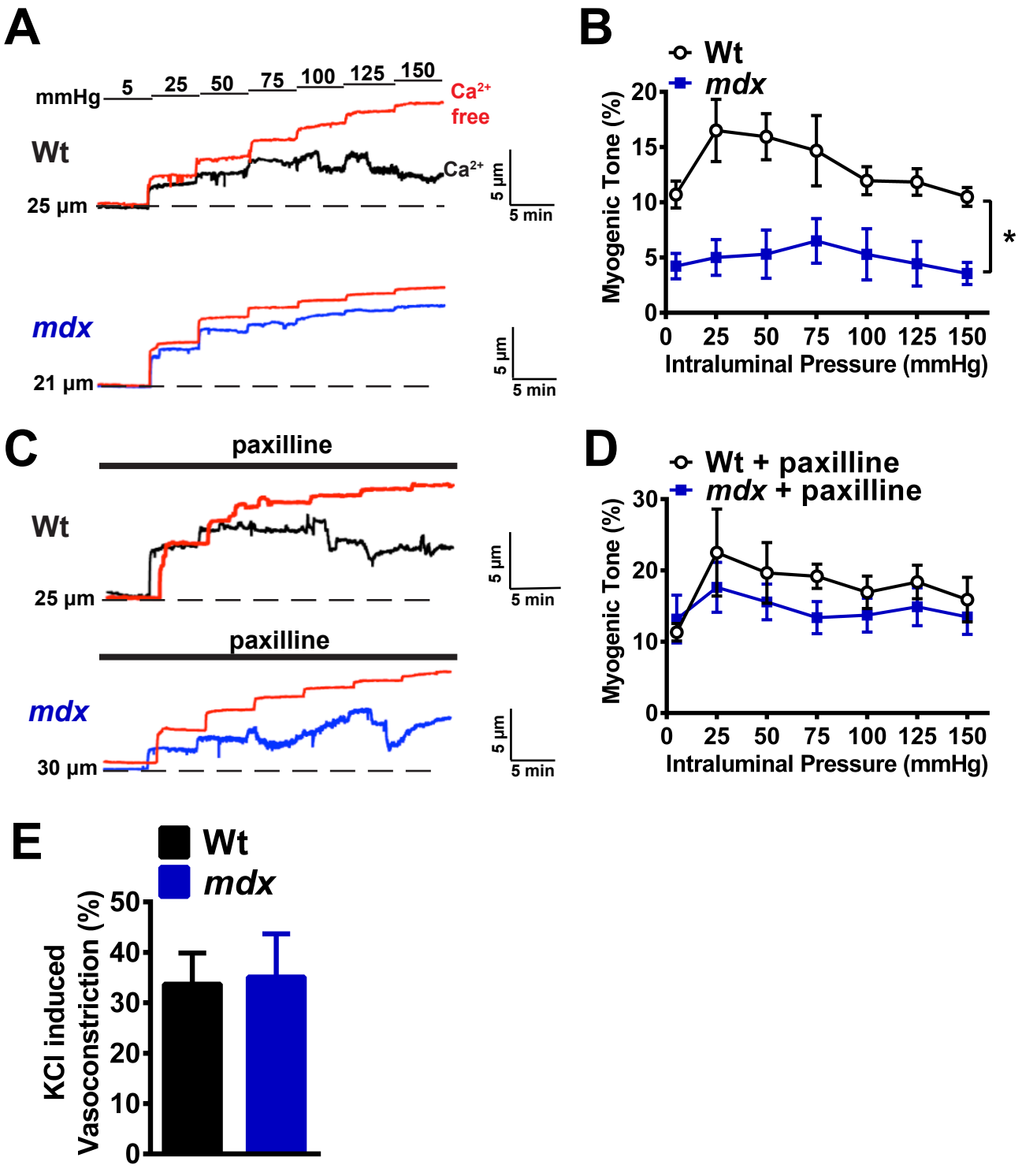

Supplemental Figure 11. Functional impairment in cerebral parenchymal arterioles from *mdx* mice. (A) Representative traces showing changes in luminal diameter over a range of intraluminal pressures (5–150 mmHg). Top panel shows a recording obtained from a cerebral parenchymal arteriole from a wild-type (Wt) mouse (black), and the lower panel shows a recording from a parenchymal arteriole from an *mdx* mouse (blue). In both panels, the passive change in diameter in response to intraluminal pressure is shown in red. (B) Myogenic tone for both groups. Myogenic tone was greater in cerebral parenchymal arterioles from Wt mice than those from *mdx* mice (n = 7-8 arterioles/group, 47-8 animals/group; *P < 0.05). (C) Similar experiment to that shown in panel A, except in the presence of paxilline (1 µM). (D) Mean myogenic tone of both groups in the presence of paxilline (n = 7 arterioles/group, 4 animals/group). There were no significant differences.(E) Constriction of isolated cerebral parenchymal arterioles from Wt and *mdx* mice in response to elevated extracellular [K^+] (60 mM). There were no significant differences.

SUPPLEMENTAL METHODS

Cluster size distribution analysis: Cluster size distribution was analyzed using the open-source CellProfiler (v. 3.0.0) software package (1). For this analysis, 50 rectangular subimages of 50 × 50 pixels were generated for each super-resolution map using NIH ImageJ (v. 2.0.0). These subimages were uploaded into CellProfile, split into individual channels for Alexa555 and Alexa647 and converted to greyscale images. A minimal threshold correction factor was applied to remove background from the subimage and the number of pixels occupied by each cluster was determined. The area of each pixel was determined based on a scaling factor (20 x 20 nm) established by LASAF software

Object-based colocalization analysis: Object-based analysis was used to establish colocalization of BKα channels and RyR2s in super-resolution localization maps. For this analysis, we used NIH ImageJ software with the JACoP colocalization analysis plug-in (2, 3). Super-resolution localization maps were divided into a series of subimages of equal area before analysis. The JACoP plug-in was used to split the red and green channels representing fluorophores detected by Alexa Fluor555 or Alexa Fluor647, respectively. Contiguous objects in both channels were identified by systematically inspecting the neighboring 8 pixels (in 2D) of a reference pixel. All adjacent pixels with intensities above a user defined threshold limit were considered to be part of the same structure as the reference pixel and were segmented as individual objects. The super-resolution localization maps were previously thresholded by the detection algorithm incorporated into the LASAF software used for image acquisition. Therefore, the threshold level in JACoP was set to 2 (nearly the minimum) for all images. After segmentation and thresholding, centroids, defined as the single-pixel geometric centers of the defined objects, were determined for each object, and the distance between centroids was measured for objects labeled with Alexa Fluor555 or Alexa Fluor647. Centroids that occupied that same 2D space as clusters in the other wavelength were considered as "colocalized". The frequency of co-localizing clusters in the super-resolution maps was compared with simulations of randomly distributed clusters. For random simulations, subimage area was kept constant within the area of the corresponding super-resolution maps. The parameters selected for the Coste's randomization process within Image J were selected to generate images with a cluster size distribution and density similar to the corresponding map. Co-localizing RyR2-BK clusters that were identified using object-based analyses were segregated for further cluster-size analysis.

References Cited:

1. Carpenter AE*, et al.* (2006) CellProfiler: image analysis software for identifying and quantifying cell phenotypes. *Genome biology* 7(10):R100.
2. Lachmanovich E*, et al.* (2003) Co-localization analysis of complex formation among membrane proteins by computerized fluorescence microscopy: application to immunofluorescence co-patching studies. *Journal of microscopy* 212(Pt 2):122-131.
3. Bolte S & Cordelieres FP (2006) A guided tour into subcellular colocalization analysis in light microscopy. *Journal of microscopy* 224(Pt 3):213-232.